on which this core velocity is zero, provided that $1 \le r_v \le R$. On manipulation of these inequalities we find that the zero-order core velocity is zero when

$$\frac{3R^2}{2 + 3R^2 + R^3} \le T_i \le \frac{1 + 2R^3}{1 + 3R + 2R^3} \tag{12}$$

which, for example, reduces to

$$\begin{array}{ll} R \to \infty & 0 \le T_i \le 1 \\ R = 4 & \frac{12}{57} \le T_i \le \frac{65}{77} \\ R = 2 & \frac{6}{11} \le T_i \le \frac{17}{23} \\ R = \frac{3}{2} & \frac{54}{97} \le T_i \le \frac{31}{49} \\ R \to 1 & T_i = \frac{1}{2} \end{array} \tag{13}$$

Therefore, there is a finite range of values of T_i for which the zero-order core velocity is zero for all values of R, but as $R \to 1$, $T_i \to \frac{1}{2}$.

It is observed from all (i) in Fig. 1, that as $t^* \to 0$, the boundary layers on $r = 1$ and $r = R$ are of zero thickness, and then as t^* increases, these boundary layers increase in thickness and diffuse into the core flow. Furthermore, it is seen that when $T_i = 1$ ($T_i = 0$), i.e., $T_o = 0$ ($T_i = -1$), then the boundary layer on the outer (inner) sphere has not been changed from that of the original core temperature.

References

[1]Cheng, P., "Geothermal Heat Transfer," *Handbook of Heat Transfer Applications*, edited by W. M. Rohsenow, J. P. Hartnett, and E. N. Ganic, 2nd ed., McGraw-Hill, New York, 1985, Chap. 11.

[2]Bejan, A., "Convective Heat Transfer in Porous Media," *Handbook of Single-Phase Convective Heat Transfer*, edited by S. Kakac, R. K. Shah, and W. Aung, Wiley, New York, 1987, Chap. 16.

[3]Caltagirone, J. P., "Thermoconvective Instabilities in a Porous Medium Bounded by Two Concentric Horizontal Cylinders," *Journal of Fluid Mechanics*, Vol. 76, Pt. 2, 1976, pp. 337–362.

[4]Bejan, A., and Tien, C. L., "Natural Convection in Horizontal Cylinders with Different End Temperatures," *International Journal of Heat and Mass Transfer*, Vol. 22, No. 6, 1979, pp. 919–927.

[5]Havstad, M. A., and Burns, P. J., "Convective Heat Transfer in Vertical Cylindrical Annuli Filled with a Porous Medium," *International Journal of Heat and Mass Transfer*, Vol. 25, No. 11, 1982, pp. 1755–1765.

[6]Vasseur, P., Nguyen, T. H., Robilard, L., and Thi, V. K. T., "Natural Convection Between Horizontal Concentric Cylinders Filled with a Porous Layer with Internal Heat Generation," *International Journal of Heat and Mass Transfer*, Vol. 27, No. 3, 1984, pp. 337–349.

[7]Bau, H. H., "Low Rayleigh Number Thermal Convection in a Saturated Porous Medium Bounded by Two Horizontal, Eccentric Cylinders," *Journal of Heat Transfer*, Vol. 106, No. 1, 1984, pp. 166–175.

[8]Himasekhar, K., and Bau, H. H., "Two Dimensional Bifurcation Phenomena in Thermal Convection in Horizontal, Concentric Annuli Containing Saturated Porous Media," *Journal of Fluid Mechanics*, Vol. 187, Pt. 2, 1988, pp. 267–300.

[9]Kimura, S., and Pop, I., "Conjugate Natural Convection Between Horizontal Concentric Cylinders Filled with a Porous Medium," *Wärme- und Stoffübertragung*, Vol. 27, No. 1, 1992, pp. 85–91.

[10]Burns, J. P., and Tien, C. L., "Natural Convection in Porous Media Bounded by Concentric Spheres and Horizontal Cylinders," *International Journal of Heat and Mass Transfer*, Vol. 22, No. 6, 1979, pp. 929–939.

[11]Sano, T., "Transient Natural Convection Between Horizontal Concentric Cylinders," *Fluid Dynamics Research*, Vol. 1, No. 1, 1986, pp. 33–47.

[12]Pop, I., Ingham, D. B., and Cheng, P., "Transient Natural Convection in a Horizontal Concentric Annulus Filled with a Porous Medium," *Journal of Heat Transfer*, Vol. 114, No. 4, 1992, pp. 990–997.

Calculation of Real-Gas Effects on Airfoil Aerodynamic Characteristics

Chul Park*
NASA Ames Research Center, Moffett Field, California 94035
and
Seokkwan Yoon†
MCAT Institute, Moffett Field, California 94035

Nomenclature

a/a = angle of attack, deg
C_D = drag coefficient
C_L = lift coefficient
CP = center of pressure
V = flight velocity, km/s
γ = specific heat ratio

Introduction

ELLIPSES of thickness ratio varying from 5 to 15% and the airfoil for the wings of the Space Shuttle Orbiter are considered for this study. Their exact geometries are given in Ref. 1. Chord lengths for these geometries are varied between 2–50 m. Two-dimensional, chemically reacting flowfields around these geometries are calculated in the present work using the computer codes CENS2H and CENS2D described in Refs. 2 and 3. The CENS2H code assumes air to consist of five neutral species N, O, NO, N_2, and O_2, and accounts for thermal and chemical nonequilibria in the shock layer, i.e., it uses a two-temperature reaction model. The CENS2D code is for an ideal gas of fixed γ ($=C_p/C_v$). Freestream velocity is varied between 3–7 km/s for the present calculation. The freestream density is varied as 8×10^{-6}, 4×10^{-5}, 2×10^{-4}, and 10^{-3} kg/m^3, corresponding approximately to the flight altitudes of 85, 74, 63, and 50 km, respectively. Angle of attack is varied as 20, 30, and 40 deg. The rate parameters given in Refs. 2 and 3, which are to be referred to as the standard rates, are used in most of the present calculations.

Convergence performance of these codes has been examined in Refs. 2 and 3 for an Apollo-shaped blunt body and a slender ellipse, respectively. One-temperature solutions can be obtained using CENS2H by setting the vibrational relaxation times to be very short.[2,3] Near equilibrium solutions can be obtained also using CENS2H by setting reaction rates to be very large.[2,3] It was shown in Ref. 2 that the aerodynamic characteristics of near-equilibrium flows can be represented approximately by those of ideal-gas flows of fixed γ less than 1.4.

Algebraically-generated grids of $110 \times 80 = 8800$ node points are used for the present calculations. Lift, drag, and moments are calculated accounting only for pressure, neglecting skin friction. The shift in the CP location is determined as the difference between the location of the CP for the reacting flow and that of the perfect-gas ($\gamma = 1.4$) flow. CP shift is represented as a percentage of the chord length.

Presented as Paper 90-1712 at the AIAA/ASME 5th Joint Thermophysics and Heat Transfer Conference, Seattle, WA, June 18–20, 1990; received Feb. 7, 1991; revision received Oct. 16, 1992; accepted for publication Nov. 18, 1992.

*Chief, Experimental Aerothermodynamics Section. Associate Fellow AIAA.
†Senior Scientist. Senior Member AIAA.

Results

In Fig. 1, the aerodynamic parameters calculated by the two-temperature nonequilibrium model and the constant γ model are shown for the Space Shuttle airfoil of 10-m chord length at the altitude of 74 km, flight velocity of 7 km/s, and angle of attack of 40 deg. The figure shows that the lift and drag coefficients obtained using the two-temperature reacting flow method are identical to those obtained for the ideal gas with $\gamma = 1.2$. However, the CP shift is substantially different between the two cases. Though not shown, a similar comparison was made between the two-temperature and the one-temperature calculations.[1] The calculations were for the 10-m-long, 10% ellipse for the flight altitude of 85 km, velocity of 7 km/s, and angle of attack of 40 deg. The results showed that one-temperature calculation results in a CP shift 13% smaller than that from the two-temperature calculation.

In Table 1, aerodynamic parameters are shown for different chord lengths, but with the same chord length-density product. The calculation is for the flight velocity of 7 km/s and angle of attack of 40 deg. As seen in Table 1, the aerodynamic parameters are virtually the same between the cases of different chord lengths, but the same length density products. That is, a binary scaling exists between size and density. Though not shown, comparison is also made between the solutions obtained with different rate coefficients, for the altitude of 50 km, 10% ellipse at an angle of attack of 20 deg, at the flight velocity of 3 km/s.[1] An appreciable difference was seen in the resulting aerodynamic characteristics between the two cases, even at 3 km/s.

In Fig. 2, the changes in lift and drag coefficients due to the real-gas effects are shown for the altitude of 74 km at an angle of attack of 40 deg, for the 10-m-long ellipses of three different thicknesses. Plotted here are the ratios between the C_L and C_D for the two-temperature reacting flows and those for the frozen ($\gamma = 1.4$) flows. As the figure shows, the ratios of C_L and C_D both decrease as the flight velocity increases. Though not shown, comparison was also made among the different angles of attack, for the 10%, 10-m-long ellipse for the altitudes of 50 and 74 km.[1] It was seen that C_L and C_D begin to deviate from the perfect-gas values at the flight velocity of 3 km/s.

Table 1 Aerodynamic parameters for the different size airfoils with the same chord length-density products

Chord length, m	Freestream density, kg/m³	C_L	C_D	CP Shift, %
50	4×10^{-5}	0.6353	0.5908	0.734
10	2×10^{-4}	0.6358	0.5912	0.724
2	2×10^{-5}	0.6719	0.6222	0.651
10	8×10^{-6}	0.6703	0.6223	0.669

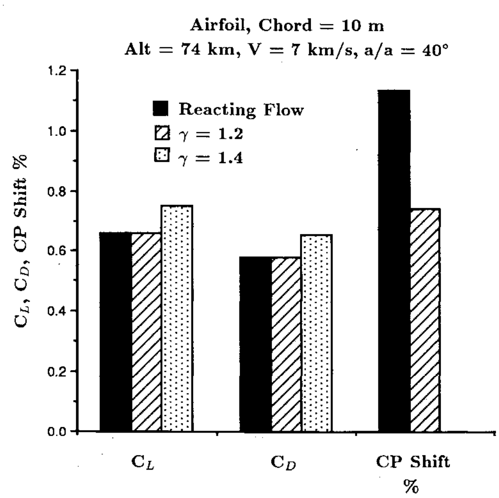

Fig. 1 C_L, C_D, and CP Shift for the Shuttle airfoil, calculated with the two-temperature reacting flow model and the constant γ model, for the chord length of 10 m, altitude of 74 km, V = 7 km/s, a/a = 40 deg.

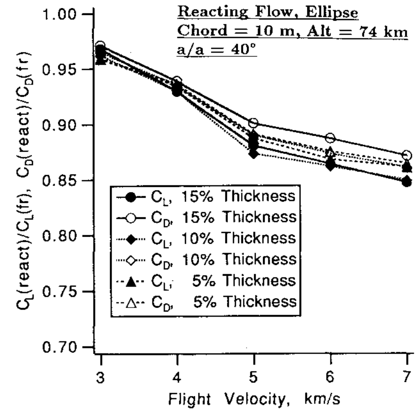

Fig. 2 Fractional changes in C_L and C_D due to the real-gas effects calculated for the ellipses of 5, 10, and 15% thicknesses, as functions of V, for the chord length of 10 m, altitude of 74 km, a/a = 40 deg.

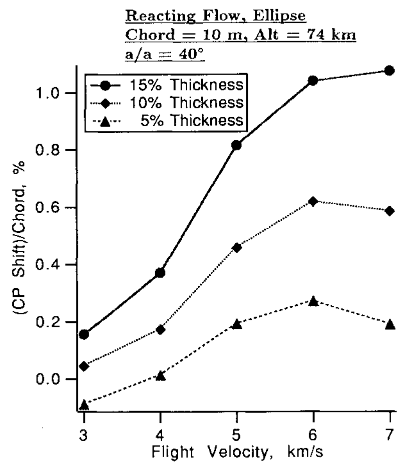

Fig. 3 CP Shift due to real-gas effects for the ellipses of 5, 10, and 15% thicknesses as a function of V, for the chord length of 10 m, altitude of 74 km, and a/a = 40 deg.

In Fig. 3, forward shift of CP location is shown for the three ellipses at the flight altitude of 74 km and angle of attack of 40 deg. As seen in the figure, CP shift is a fairly strong function of thickness ratio. CP shift generally increases with flight velocity. However, between 6–7 km/s, the trend reverses. In Fig. 4, CP shift is shown for the three calculated flight altitudes, for the 10%, 10-m-long ellipse. The figure shows that CP shift is only weakly affected by flight altitude, at least over the range considered. It generally increases with increase in flight velocity, but remains nearly constant between 6–7 km/s, at least for the angle of attack of 40 deg.

A near-equilibrium solution is obtained by setting all reaction rate coefficients to be 10 times the standard values. The calculation is made for a 10% ellipse at an angle of attack of 20 deg for an altitude of 50 km and flight velocity of 3 km/s. The result is compared with the standard case and the perfect-gas case in Table 2. As seen in the Table, the near-equilibrium solution yields C_L and C_D values that are little different from those of the standard case. But its CP shift is considerably smaller. This trend is the same as that seen in Fig. 1, which shows the $\gamma = 1.2$ solution producing a smaller CP shift than the reacting flow solution.

Reference 1 contains other solutions not mentioned here, but reinforces the points made in this Note. There are no two-dimensional experimental data with which the present calculations can be compared. However, during the entry flights of the Shuttle vehicles, a forward CP shift of the order

Table 2 Comparison of aerodynamic characteristics between the solutions with different rate coefficients; ellipses of 10% thickness, at the altitude of 50 km and angle of attack of 20 deg

	$\gamma = 1.4$	Standard rates	Rates × 10
C_L	0.3206	0.3175	0.3090
C_D	0.1531	0.1515	0.1478
CP Shift, %	0	−0.14	−0.081

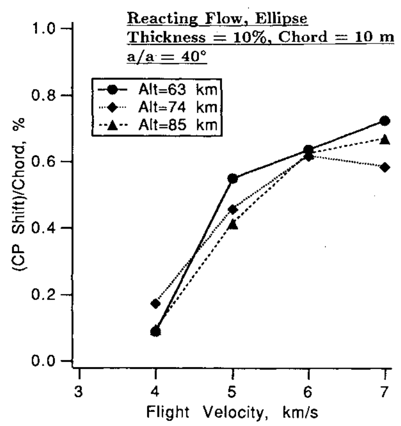

Fig. 4 CP Shift due to real-gas effects for the ellipse of 10% thickness as a function of V, for the chord length of 10 m, a/a = 40 deg, and for the altitudes of 63, 74, and 85 km.

of 0.6 ± 0.2% has been observed at angles of attack between 20–40 deg.[4] The CP shifts calculated in the present work are also of the same order.

References

[1]Park, C., and Yoon, S., "Calculation of Real-Gas Effects on Airfoil Aerodynamic Characteristics," AIAA Paper 90-1712, June 1990.

[2]Park, C., and Yoon, S., "Calculation of Real-Gas Effects on Blunt-Body Trim Angles," *AIAA Journal*, Vol. 30, No. 4, 1992, pp. 999–1007.

[3]Park, C., and Yoon, S., "Fully Coupled Implicit Method for Thermochemical Nonequilibrium Air at Suborbital Flight Speeds," *Journal of Spacecraft and Rockets*, Vol. 28, No. 1, 1991, pp. 31–39.

[4]Griffith, B. J., and Maus, J. R., "Explanation of the Hypersonic Longitudinal Stability Problem—Lessons Learned," *Shuttle Performance: Lessons Learned*, NASA CP-2283, 1983, pp. 347–379.

Filmwise Condensation on Nonisothermal Horizontal Elliptical Tubes with Surface Tension

Sheng-An Yang*
National Kaohsiung Institute of Technology, Taiwan, Republic of China
and
Cha'o-Kuang Chen†
National Cheng-Kung University, Taiwan, Republic of China

Received Aug. 7, 1992; revision received Dec. 28, 1992; accepted for publication Dec. 29, 1992.

*Associate Professor, Department of Die-Making Engineering.
†Professor, Department of Mechanical Engineering.

Nomenclature

a, b	=	semimajor, semiminor axis of ellipse
C_p	=	specific heat of condensate at constant pressure
g	=	acceleration due to gravity
$h, \bar{h}$	=	local, mean condensing heat transfer coefficient
k	=	thermal conductivity of condensate
Pr	=	Prandtl number
x, y	=	coordinate measuring length along circumference from top of tube, normal to x
μ	=	absolute viscosity of condensate
ρ, ρ_v	=	density of condensate, vapor
σ	=	surface tension coefficient in the film

I. Introduction

THE origin Nusselt[1] model for filmwise condensation of a quiescent vapor along an isothermal vertical plate equated gravity and viscous forces and assumed a linear temperature profile across the condensate layer. Nusselt did not consider film acceleration and energy convection effects. Afterward, many investigators, such as Rohsenow,[2] Churchill,[3] and Memory and Rose[4] have directed their effort at studying the impact of Nusselt's assumptions under such conditions and made significant improvements on Nusselt condensation theory.

Our major aim of this Note is intended to help the easy use of the Nusselt-Rohsenow-type condensation analysis with further account for the effect of surface tension by developing analytical, explicit, and straightforward integrating solutions for the problem of laminar-film condensation onto horizontal elliptical tubes, including vertical plates and horizontal circular tubes, under wall temperature variations.

II. Analysis

Consider a horizontal elliptical tube with its major axis "$2a$" oriented in the direction of gravity, situated in a quiescent pure vapor which is at its saturation temperature T_{sat}. The wall temperature T_w is nonuniform and below the saturation temperature. Thus, condensation occurs on the wall and a

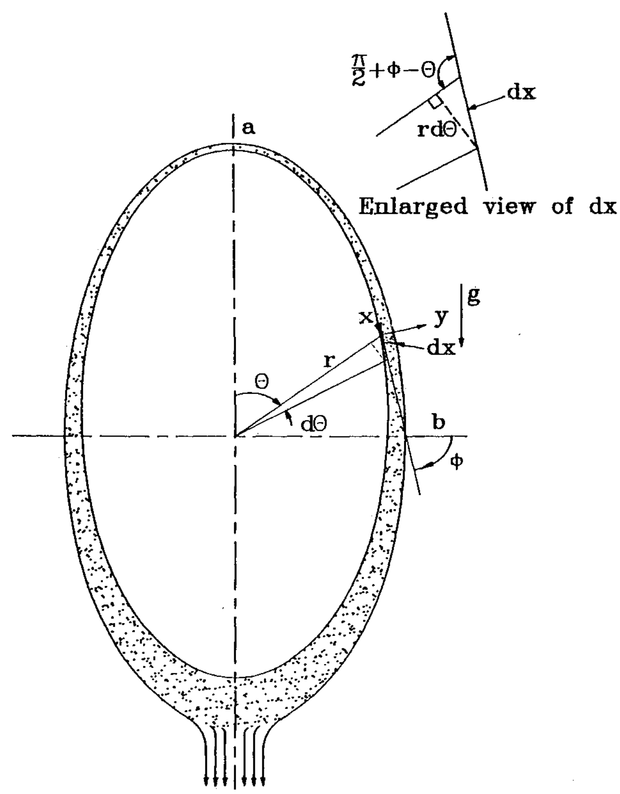

Fig. 1 Schematic and coordinate system for the condensate film flow on the elliptical surface.